Temporal Stability of Shear-Wave Anisotropy in the Vicinity of the Joshua Tree - Landers Earthquake Sequence

George W. Slad
Earth and Environmental Science Department
New Mexico Institute of Mining and Technology
Socorro, NM 87801

Submitted in partial fulfillment of the requirements for the Degree, Master of Science in Geophysics from the Department of Earth and Environmental Science, New Mexico Institute of Mining and Technology.

May 1, 1996

Abstract

Prior to the Landers earthquake, observed shear-wave anisotropy from local microearthquakes recorded at a 3-component Southern California Seismic Network station, approximately 20 km south of the Landers mainshock and 5 km west of the Joshua Tree mainshock, has an initial S-wave polarization azimuth of 14° E of true N. This analysis indicated stable S_{fast} polarization azimuth preceding the Joshua Tree - Landers earthquake sequence. Following the Landers earthquake we observed an apparently progressive 30° rotation to the E of the initial shear-wave polarization azimuth. However, residual initial P-wave polarization azimuths from local and regional earthquakes indicate that the horizontal components of the seismometer were reoriented approximately 30° to the W in mid-1993 during site maintenance. After correcting for the reorientation of the horizontal components of the seismometer, the trend in S_{fast} azimuths largely disappears and is suggestive of temporal stability in crustal anisotropy, despite the close proximity of the earthquake sequence and associated deviatoric stress change. Differential analysis of shear-waves from similar microearthquake pairs with temporal separations of ~2 to 3 years was also employed to constrain a possible temporal change. This analysis yielded no detectable co- or post-Landers (or post-Joshua Tree) changes in shear-wave anisotropy azimuths or splitting interval at levels of $0.29 \pm 0.21 \times 10^{-2} s$ for five such pairs, each spanning more than 1.8 years of post-Joshua Tree and Landers seismicity.

Table of Contents

Abstract i

Table of Contents ii

List of Figures iii

List of Tables iv

Motivation 1

Conventional Dilatancy 2

Extensive Dilatancy Anisotropy 4

Study Area 5

Polarization Analysis 9

Similar Event Analysis 14

Discussion and Conclusion 23

Acknowledgments 25

References 26

List of Appendices 29

List of Figures

Figure 1. Regional View of southern California 6

Figure 2. Timeline of Seismicity of Study Area and Study Area 8

Figure 3. Initial Shear-Wave Polarization Azimuths 11

Figure 4. Initial Compressional-Wave Polarization Residual Azimuths 12

Figure 5. Inferred Horizontal Seismometer Orientation 13

Figure 6. Similar Microearthquake Seismograms 15

Figure 7. Shear-Wave Differential Analysis 17

Figure 8. Compressional-Wave Differential Analysis 19

Figure 9. Shear-Wave Comparison 21

Figure 10. Seismogram Comparison Before and After Correction 22

List of Tables

Table 1. Velocity Models 16

Table 2. Differential Analysis Results 20

Motivation

Crustal shear-wave anisotropy has been observed in numerous areas through-out the world (e.g., Savage, et al., 1989, Vázquez-Contreras, et al., 1993, Munson, et al., 1995). However, temporal changes in anisotropy associated with the earthquake stress buildup and relaxation cycle, although proposed have not yet been conclusively demonstrated. For example, results can be skewed by subjective estimates of polarization and shear-wave splitting times. Several papers on shear-wave anisotropy and earthquake prediction are evidence of the controversial nature of observed temporal shear-wave anisotropy changes associated with earthquakes (e.g., Peacock, et al., 1988; Crampin et al., 1990,1991; Aster et al., 1990, 1991).

The Joshua Tree - Landers earthquake sequence began with the M_w=6.1 Joshua Tree earthquake, which had an average stress drop estimated at 20-40 bars (Bennett, et. al., 1995). On June 28, 1992 southern California experienced the M_w= 7.3 Landers earthquake, the largest earthquake since the Kern County earthquake of 1952 (M=7.5)(Campbell and Bozorgnia, 1994). This earthquake was especially notable for remotely triggering seismicity and affecting geyser activity as far away as the Yellowstone region (Hill, et al., 1993). The average stress drop associated with the Landers earthquake has been estimated at 35 bars (King, et. al., 1994). The Joshua Tree - Landers earthquake sequence is, quite arguably, the best opportunity presently available for searching for temporal changes in shear-wave anisotropy associated with large shallow earthquakes in the United States. Here I present a comprehensive study of shear-wave anisotropy in the shallow crust approximately 20 km south of the Landers mainshock epicenter and 5 km west

of the Joshua Tree mainshock epicenter.

Conventional Dilatancy

Hubburt and Willis (1957), in the laboratory, showed that rock fractures formed parallel to the maximum compressive stress, σ_{max} and opened perpendicular to the minimum compressive stress, σ_{min}. Evidence in the field has also been cited [Hubburt and Willis, 1957]. Spanish Peaks, a pair of mountains east of the Culebra Range in southern Colorado exhibits this principle of cracks opening parallel to maximum compressive stress [Odé, 1957]. The peaks are the ancient conduit that fed a dike system intruding into the surrounding rock. As these vertical conduits intruded, a radial stress emanating from the center, became the principal compressive stress in the vicinity of the intrusion. Fractures opened parallel to the radiating stress pattern, which in turn filled with magma forming a radiating pattern of igneous dikes. Further from the vertical pipe where the dike radial stresses diminish, the dikes divert from the radiating pattern, into segments paralleling the regional east-west maximum compressive stress. Today the oil and gas industry, and more pertinent to this paper, the seismological community, utilize the principles of fracture orientation in numerous applications.

Dilatancy is the nonelastic volume increase due to a void space increase in rocks through the development of microcracks resulting from the application of a deviatoric stress (Scholtz, 1990). Rock mechanicists have shown that dilatancy occurred in various specimens such as dolomite, marble, basalt, and granite exhibit dilatancy in laboratory experiments under confining pressure [Brace, 1966]. With repeated demonstration of rock samples exhibiting dilatancy in the lab, seis-

mologists looked to the earth to search for possible variations in body wave velocities induced by stress changes associated with the earthquake cycle. The concept of relating earthquake prediction to dilatancy theory drew the attention of many seismologists and resulted in a host of publications in the early 1970's (Nur, 1972, Gupta, 1973, Whitcomb, 1973).

Early earthquake prediction papers concentrated on variations in P to S velocity ratios. Difficulties soon emerged with defining what P to S velocity ratios measured in the field told scientists about the state of stress within the earth. Gupta (1973) studied the effect of varying the raypath azimuth on P to S velocity ratio in laboratory samples and noted that P to S velocity ratios were not constant with varying raypath azimuths relative to σ_{max}. Fault type was also shown to have a large effect on the P to S velocity ratio. The shortcomings of V_P/V_S studies led in part to the analysis of shear wave birefringence (Gupta, 1973) as a possibly more robust observable in the search for temporal variability.

Shear wave birefringence, or splitting, due to seismic anisotropy is the effect that a shear wave decomposes into two components with one component traveling slightly slower than the other in a medium with anisotropic elastic behavior. Anisotropic elasticity may result from aligned minerals in the host rock, finely bedded layers, or fluid-filled fractures or microcracks. Various minerals, such as biotite, for example are highly anisotropic due to the layered nature of their crystalline structure. We focus on the more seismically interesting splitting effect due to stress-aligned microcracks within the crust. Where the shear-wave travels through a material with anisotropic velocity characteristics two waves are created; a quasi-fast shear wave oscillating parallel to the maximum compressive stress, σ_{max}, and a quasi-slow shear wave oscillating parallel to the mini-

mum compressive stress, σ_{min}. Gupta (1973b) claimed to observe premonitory changes in shear-wave splitting before two M_L=4.0 earthquakes in Nevada. Later, however, it was pointed out that the observations could not be unambiguously attributed to shear-wave splitting, but also could be due to crustal heterogeneity and phase conversion [Ryan and Savage, 1974]. Direct shear wave velocity studies also continued during this period, and studies minimizing source and ray path differences, such as (McEvilly and Johnson, 1973, 1974) utilizing quarry blasts with raypaths near earthquake hypocenters, did not show significant variations. The theory of conventional dilatancy, the premise that V_P/V_S and early shear wave anisotropy studies are based on, also came under scrutiny, with accumulating evidence that crustal rocks near fault zones generally do not experience the high deviatoric stresses on which laboratory dilatancy results are based. In fact, deviatoric stresses that crustal rocks undergo are now considered to be far below the yield strength of intact rocks (Zoback, et. al., 1987).

Extensive Dilatancy Anisotropy

Although conventional dilatancy theory had become largely discredited as a common process in seismic regions, a new theory of dilatancy evolved that required nearly an order of magnitude less stress than that of the conventional dilatancy theory [Crampin, 1984]. The elastic dilatancy anisotropy (EDA) hypothesis does not rely on creating fractures in rock, but rather considers the effects of stress variations on microcracks already existing within the crust, or growing under low-stress conditions.

The EDA hypothesis is based on four well-documented observations. First, unjacketed laboratory rock samples subjected to low deviatoric stresses have shown preferential cracking aligned paral-

lel with σ_{max} (Nur and Simmons, 1969). Second, abundant pore fluids are known to exist several kilometers deep within the crust (Crampin, 1984). Confining pressure at these depths are very high, so in order for fluids to exist at these levels pore-fluid pressures (P_f) must be comparable to the confining pressure (P_c). Therefore the effective confining pressure (P_{eff}), where $P_{eff} = P_c - P_f$, is low. The host rock is weaker under low effective confining stress so that, when subjected to a small deviatoric stress, existing microcracks will differentially open and close (Nur and Byerlee, 1971). Third, stress-corrosion can cause subcritical crack growth parallel to σ_{max} under low strain rates and low pore-fluid pressures. For example, laboratory experiments with quartz have shown this behavior (Atkinson, 1972). Finally, the aforementioned aligned microcracks and sub-critical growth cracks are expected to create an effective anisotropic medium.

Study Area

The region studied lies approximately 17 km south of southernmost surface rupture from the $M_W = 7.3$, June 28, 1992 Landers earthquake and approximately 5 km west-southwest of the $M_W = 6.1$, April 23, 1992 Joshua Tree earthquake (Hauksson, et al., 1993; Sieh, et al., 1993; Figure 1). Clearly this region underwent a significant and nearly instantaneous stress change during 1992. Average stress drop across the fault for the Joshua Tree earthquake is estimated at 20-40 bars (Bennett, et. al., 1995). The Landers earthquake, the largest earthquake to occur in California in 40 years, had an estimated average stress drop of 35 bars (King, et. al., 1994).

To search for possible co- or post-seismic changes in shear-wave anisotropy associated with this stress reorganization, we analyzed near-vertically traveling shear-waves from microearthquakes

since April 30, 1981 recorded at the Southern California Seismic Network station East Wide Canyon (EWC; Appendix A). EWC is a three component station, consisting of L-4 seismometers, situated 466 m above sea level in an igneous and metamorphic complex in East Wide Canyon

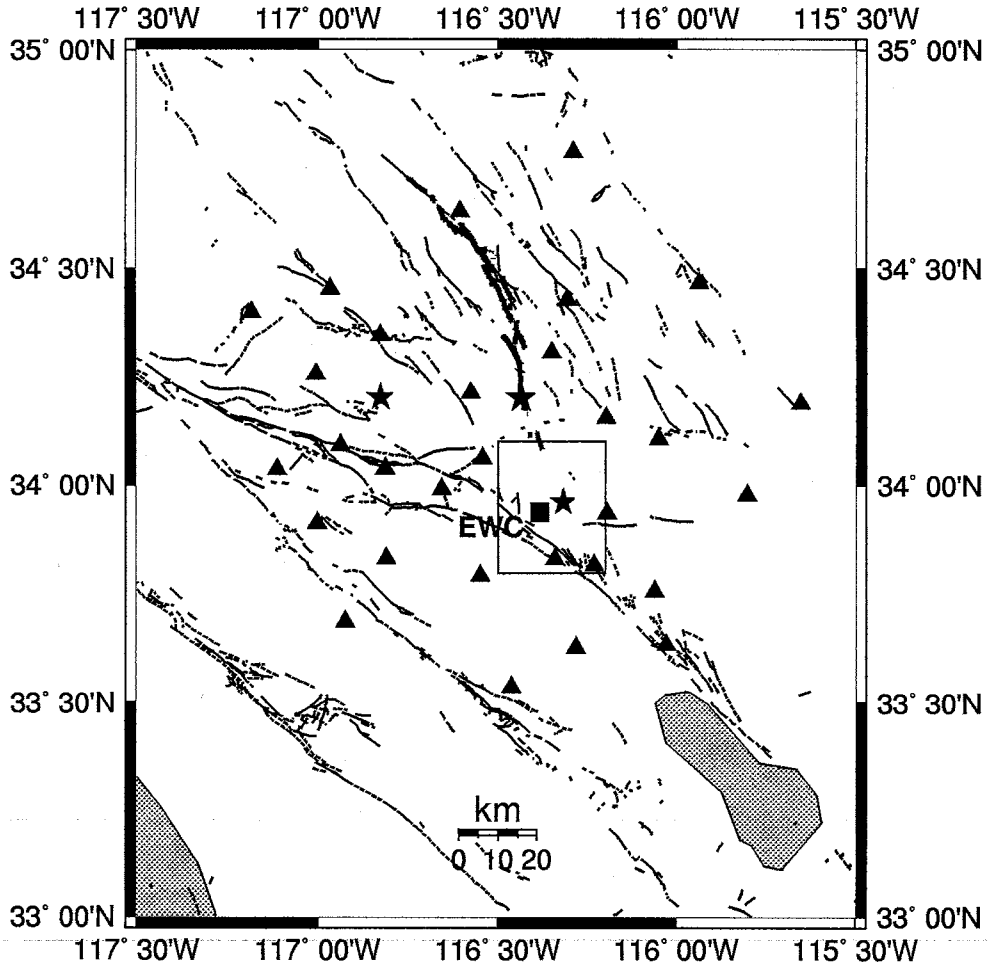

Figure 1. View of southern California showing prominent faults and mainshock and station locations. Triangles illustrate the locations of seismic stations operated and maintained by the Southern California Seismic Network (SCSN). The square represents East Wide Canyon (EWC), a three-component station in near constant operation from April 30, 1981 through February 15,1996, also maintained by the SCSN. The stars depict, counter-clockwise from bottom, the epicenters of the Joshua Tree (April 23, 1992, M_w=6.1), Landers (June 28, 1992, M_w=7.3), and Big Bear (June 28, 1992, M_w=6.5) earthquakes. The San Andreas Fault Zone trends northwest within 5 km of EWC. Thick line segments denote the mapped surface rupture (over 70 km) from the Landers earthquake. The black outlined box denotes our study area.

approximately 5 km N of the San Andreas fault zone. Data sampling rates vary from 50 to 100 samples per second for this station. The data is archived on a compact disc mass-storage system at the Southern California Earthquake Center (Hafner and Clayton, 1994). The 15-year digital record for this three-component station is one of the longest for the SCSN in southern California.

Near vertically-traveling shear waves are more amenable than lower incidence waves for obtaining measurements of shear-wave anisotropy because they are typically less contaminated by S-to-P converted phases arising at sub-horizontal interfaces or at the free surface (Booth and Crampin, 1985). We thus selected our initial data set as all events occupying a conical volume with its apex at EWC, and having a half angle of $35°$. A total of 363 events remained after excluding events with clipped waveforms, missing components, and/or high levels of instrumental noise (Figure 2a and 2b).

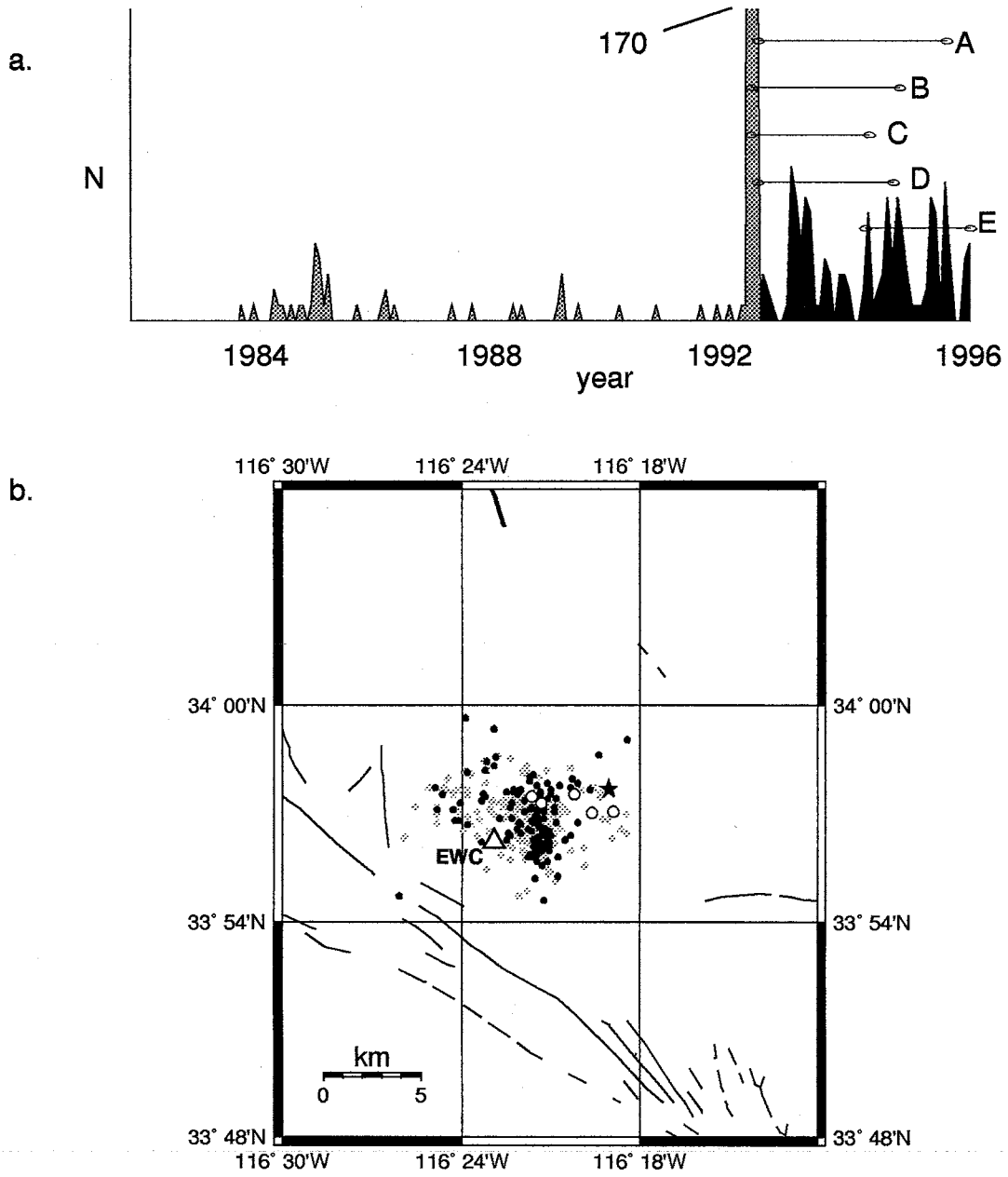

Figure 2. (a) Timeline of seismicity within the conical search volume (see text). Points connected by line segments denote similar microearthquakes used in the differential analysis (Table 2). (b) Area map of events included in this study. Grey events occurred before the Landers earthquake. The epicenters are dispersed relatively evenly throughout the search area. Events after the Landers earthquake are black. The southern-most mapped surface rupture of the Landers earthquake, the thick line segment on the very top, comes within 17 km of EWC. The black outlined circles denote the mean relocations of similar microearthquake pairs used in the differential analysis of shear wave splitting parameters.

Polarization Analysis

Crustal shear-wave anisotropy is most easily observed as a strong alignment of initial shear-wave particle motion directions independent of the shear-wave radiation patterns of the earthquake sources, due to the initially arriving energy being dominated by the fast quasi-shear wave. To measure this phenomenon for the data set examined here, we first picked the arrival times of the shear-waves and estimated the vector linearity (Aster et al., 1990) of the three-component particle motion from the covariance matrix decomposition (Kanasewich, 1975) of the initial eight samples (0.08 s) following the shear-wave arrival, where the covariance matrix of the three-component signal is

$$Cov = \begin{bmatrix} var(1,1) & cov(1,2) & cov(1,3) \\ cov(2,1) & var(2,2) & cov(2,3) \\ cov(3,1) & cov(3,2) & var(3,3) \end{bmatrix} \quad (1)$$

The degree of linearity of this particle motion segment may be simply calculated from the eigenvalues of the eigenvector-eigenvalue decomposition of the covariance matrix as

$$l = \frac{(\lambda_1 - \lambda_2)}{(\lambda_1 - \lambda_2 + \lambda_3)} \quad (2)$$

where $\lambda_1 \geq \lambda_2 \geq \lambda_3$.

The corresponding least-squares estimate of the direction of initial particle motion is that of the unit eigenvector, $\hat{e}_1$, corresponding to the largest eigenvalue, λ_1. Highly linear initial particle motions with most of their energy in the horizontal plane (a small value of the z-component of $\hat{e}_1$) come closest to approximating the expected particle motion for vertically-traveling shear waves. Figure 3a illustrates the initial shear-wave particle motion azimuth for all events with

($l \geq 0.4, e_z \leq 0.6, N = 197$) and is immediately suggestive of a progressive change in the azimuth of the initial shear-wave particle motion by approximately $35°$ since the Joshua Tree - Landers earthquake sequence. The trend becomes increasely visible as linearity requirements increase and allowance of energy in the vertical direction decreases ($l \geq 0.6, e_z \leq 0.4, N = 121$; Figure 3b), and becomes clearest for the highest quality events ($l \geq 0.8, e_z \leq 0.2, N = 48$; Figure 3c). An initial shear-wave polarization azimuth of approximately due N (all azimuths are given relative to horizontal component coordinate system north, unless otherwise indicated) before the sequence, followed by an eastward rotation to the current polarization azimuth of about $N30°E$ is observed in all cases. A host of aftershocks following the Joshua Tree and Landers earthquakes exhibit a wide variety of initial shear-wave particle motions, however with the large number of aftershocks, which vary in location, it is likely that the cause of the observed scatter is crustal scattering. A tempting suggestion from these observations is that the fast shear wave polarization axis is gradually realigning itself in the altered stress field caused by the Joshua Tree and/or Landers earthquakes with a time scale on the order of several years.

After investigation of on-line SCSN station records for EWC, which showed no changes in station configuration that would account for the observed temporal trend, we performed a calibration on the instrumental horizontal coordinate system by examining the initial particle motion of P-waves of $M_l \geq 3.5$ regional events. Such techniques are commonly used to calibrate the component orientations of borehole instruments (e.g., Aster and Shearer, 1991a), although the steep velocity gradient and increased heterogeneity of the near surface will make such determinations more difficult for surface stations (Aster and Shearer, 1991b). Calculation of the linearity and polarization direction of the P-wave is identical to the calculation for the S-wave discussed previ-

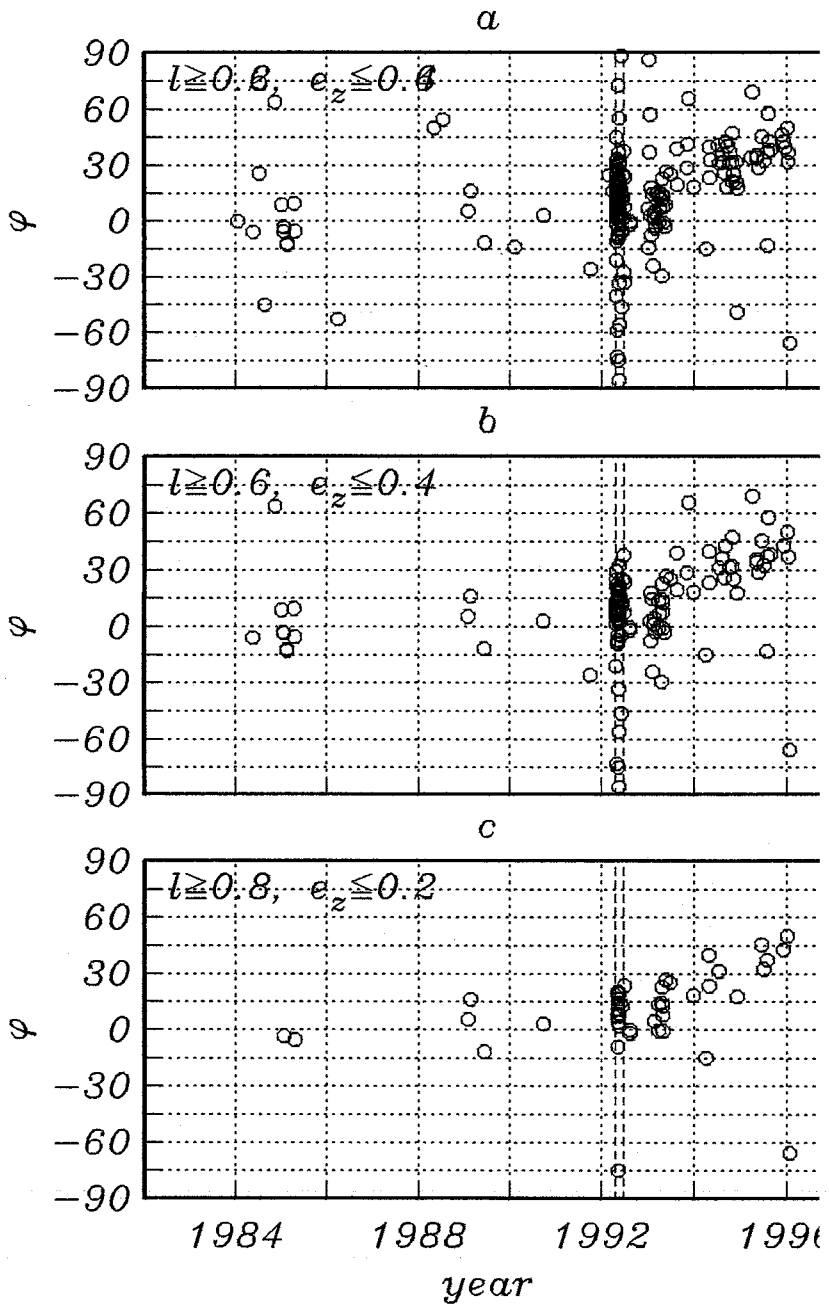

Figure 3. Shear-wave initial polarization azimuth timeline. Polarization, ϕ, ° E of N, of each initial shear- wave arrival (0.08 s of signal following the shear wave pick) is plotted as degrees east of the north component seismometer direction. Vertical lines represent the times of the Joshua Tree and Landers earthquakes. Notice the apparent progressive rotation of ϕ after the Landers earthquake.

ously. Initial horizontal P-wave particle motion azimuths are plotted as a deviation from the great circle path (GCP) in Figure 5a. Significantly, Figure 4a does not show a flat trend aligned with the great circle path (0° east of GCP) and this trend becomes clearer after further constraining the

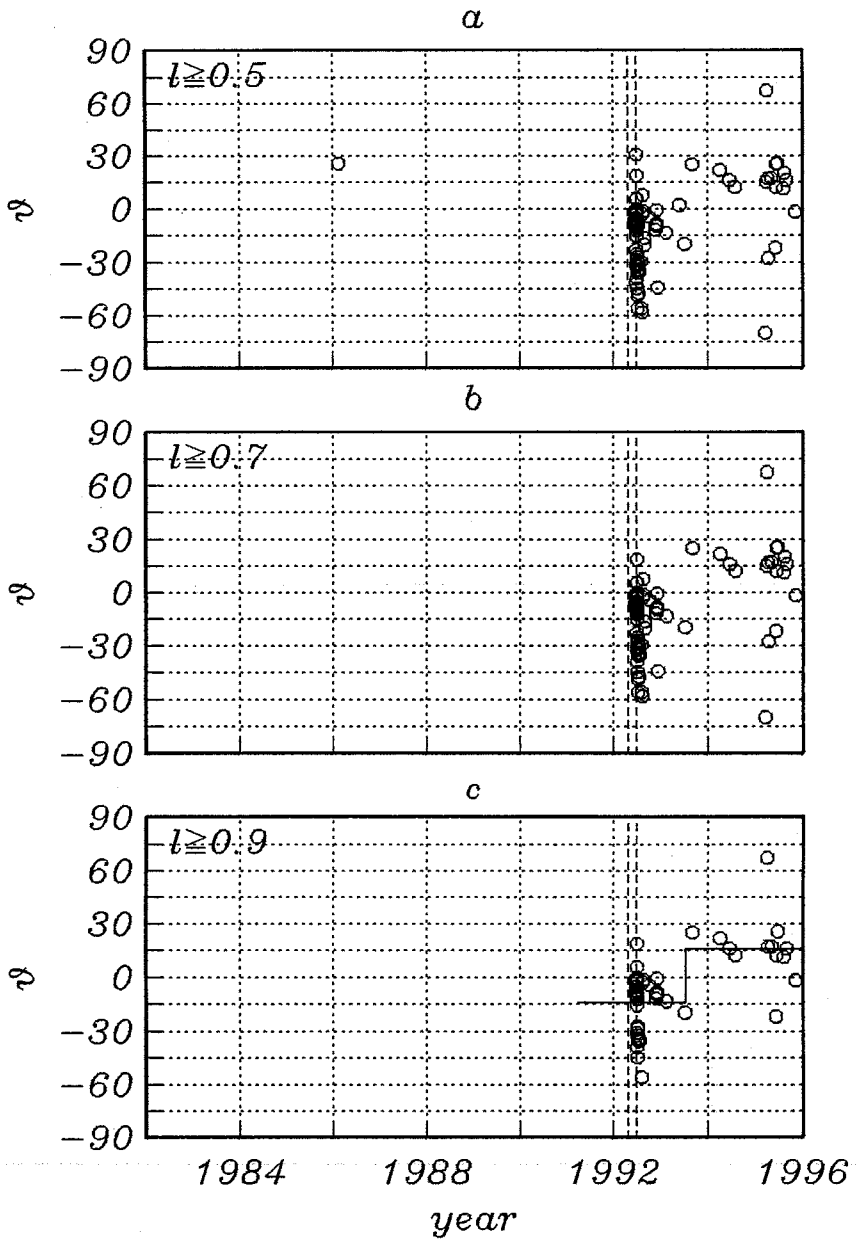

Figure 4. P-wave initial polarization residual azimuth timeline. The events shown are earthquakes with local magnitudes of at least 3.5 at ranges of 20-100 km from EWC. The polarizations are plotted in degrees east of the great circle path (GCP). The vertical, dashed lines represent the times of the Joshua Tree and Landers earthquakes. Notice the inferred abrupt shift in polarization (black line is the mean initial polarization residual azimuth before and after July 16, 1993) during mid-1993.

linearity requirements (Figures 4b and 4c). Rather, an abrupt shift in the GCP residual is observed in mid-1993. Before this shift, the mean of the highest quality events yields a polarization of 14° east of GCP. This offset corresponds to magnetic north for the area and it is reasonable to assume that the N component seismometer was installed in this orientation, rather than being

aligned to true N (L. Wald, pers. commun). After the mid-1993 shift in P-wave initial particle motion azimuth the average polarization is 16° west of GCP. The approximate 30° rotation of P-wave initial particle motion azimuths relative to great circle path has serious implications regarding the observed rotation of the quasi-fast shear-wave polarization, as it implies a reorientation of the horizontal components of the station during 1993. We were able to constrain the change in orientation as occurring sometime between July 8, 1993 and September 6, 1993 (Figure 5) by noting the dates of the microearthquakes spanning the apparent shift in Figure 4c. During the interval between earthquakes that constrain the time of the coordinate system change, EWC had 3 site visits, leaving open the possibility of an erroneous adjustment and/or a lack of complete records.

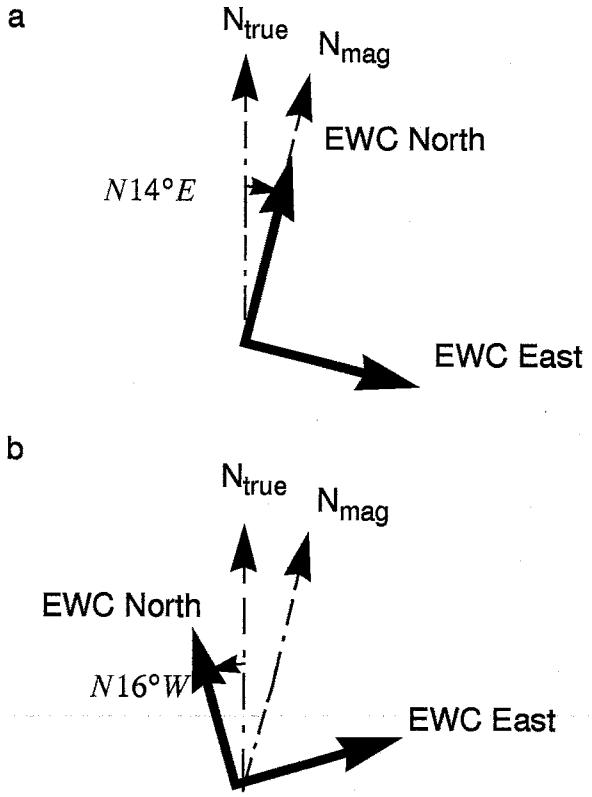

Figure 5. Inferred horizontal seismometer orientations based on P-wave polarization measurements (Figure 4). Prior to mid-1993 the horizontal components were oriented approximately $14 \pm 15°$ east of true north. This angle coincides with magnetic north for the area. After a station visit in mid-1993 in which the horizontal components were apparently redeployed with the north component oriented to $16 \pm 7°$ west of true north.

Similar Event Analysis

Differential analysis of similar microearthquakes provides a high-resolution method for detecting subtle changes in waveforms that may reflect changes in the seismic Green function (Antolik, et. al., 1996, Aster, et. al., 1990, 1991a, 1995, Nadeau, et. al., 1995). Waveform similarity is an indication of small differences in source mechanism, location, and raypath. To obtain a catalog of similar events within our conical search volume, we calculated the cross-correlation of the P-pick for approximately 1 second of data, (31 samples prior to, 96 samples after the P-pick for 100 hz data) across all common stations. The median peak cross-correlation was chosen as the similarity measure so that stations with anomalously low (typically caused by instrumental difficulties, high noise, or highly inconsistent picks) or high (typically caused by strong local site effects) cross-correlations would not bias the similarity measure. The analysis yielded four microearthquake pairs of exceptional similarity, with the first member predating and the second member postdating the Landers earthquake, with a peak median P-wave cross-correlation of at least 0.75 (Table 1). I first discuss results from one pair of microearthquakes (Table 1, pair A) with a median peak cross-correlation of 0.811 (Figures 3, 7) across 6 stations.

I relocated the four pairs of similar microearthquakes spanning the Landers earthquake. As picking the arrival times of seismic waves is a subjective process, poor signal to noise ratios, weak or emergent arrivals also inhibit consistent picks through out a dataset. Inconsistent picks and the subjectivity of the picking process may consequently lead to relatively large errors in location. To avoid this source of error, I repicked the P-wave arrivals of a subset of events within the conical volume using Xadjust, a set of sophisticated interactive programs that picks P and/or S arrivals based on waveform similarity (Dodge, 1995; see Appendix B). With the revised picks, I simulta-

neously inverted, starting with the Landers model of Hauksson et. al. (1992), for a local 1-d velocity model, (Table 1), and revised locations using the program Velest (Ellsworth, 1978). These relocations confirmed that the similar microearthquake pairs are nearly colocated, with inter-event distances ranging from ~50 meters to ~700 meters and errors less than 250 meters (horizontal and vertical).

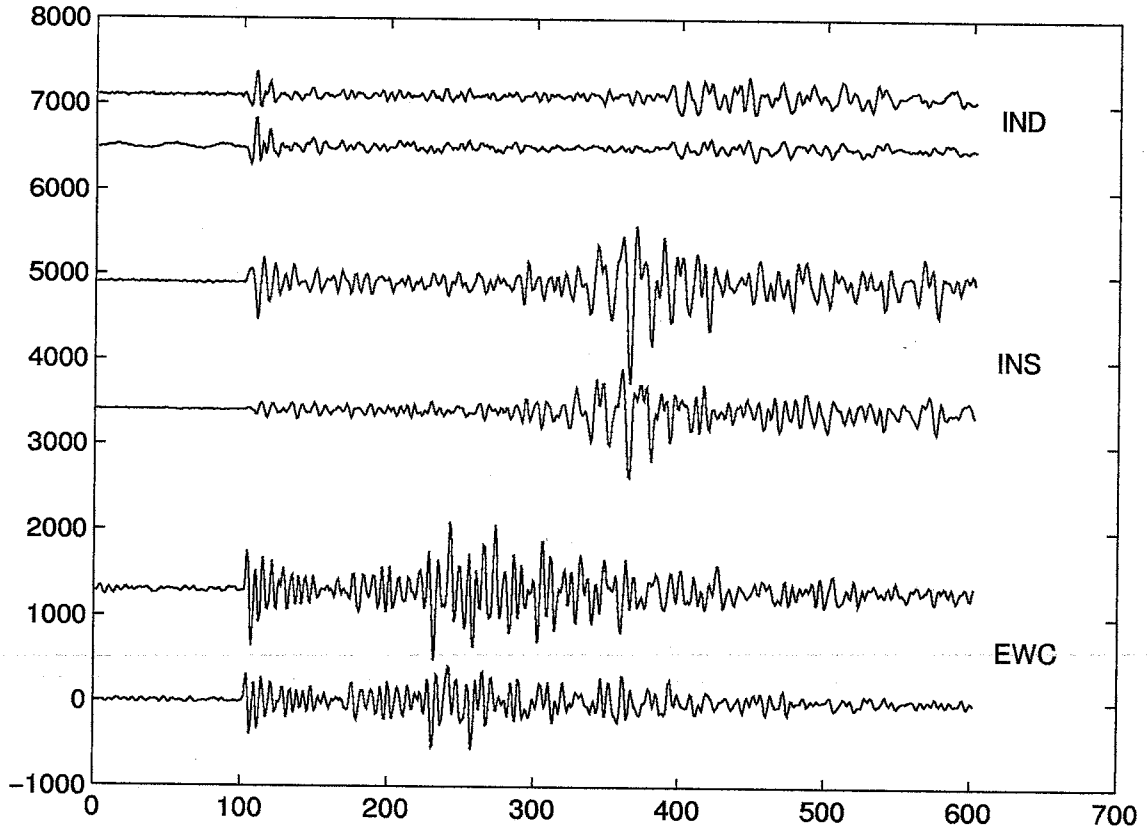

Figure 6. Seismograms of three selected stations of similar event pair A (see Table 1). The upper trace of each station is from the event which occurred on August 12, 1995, just prior to the Landers mainshock. The lower trace of each station is from the event which took place on June 26, 1992.

Table 1: Velocity Models

Depth, km	Initial Model, km/s	Refined Model, km/s
0.00	4.54	4.56
2.00	5.84	5.81
5.50	6.13	6.15
16.00	6.56	6.56
32.00	7.80	7.80

A higher resolution method of quantifying the apparent rotation of the horizontal components observed in the initial P-wave particle motions (Figure 4), is to calculate a 2-component cross-correlation measure of the similar event pair as the horizontal components of one event are rotated relative to the horizontal components of the other event. We first rotate both events, relative to their respective coordinate systems, to the orientation (S_{fast}, S_{slow}) that maximizes the shear-wave splitting prior to the 1992 event $(N7.5°E)$. In increments of 1°, from -90° to 90°, the cross-correlation function is calculated for the S_{fast} and the S_{slow} directions and Fourier interpolated to 1/64 of a sample. We average the cross-correlation functions of the S_{fast} and S_{slow} components and find the maximum of that average (which we refer to as the peak composite cross-correlation) to assess the 2-component similarity between the events. Only when both the S_{fast} and S_{slow} correlation functions are highly similar does the peak composite cross-correlation have a high value (Figure 7a). The maximum peak composite cross-correlation occurs when the 1995 event is rotated 33° west of the 1992 event. This angle remained stable (±1°) with varying window lengths (16 -128 samples) and is consistent with the coordinate system change inferred in Figure

6. The cross-correlation best lag times of S_{fast} and S_{slow} and the composite lag time are plotted in Figure 7b. The difference in the S_{fast} and S_{slow} correlation lags (the differential lag) is plotted in

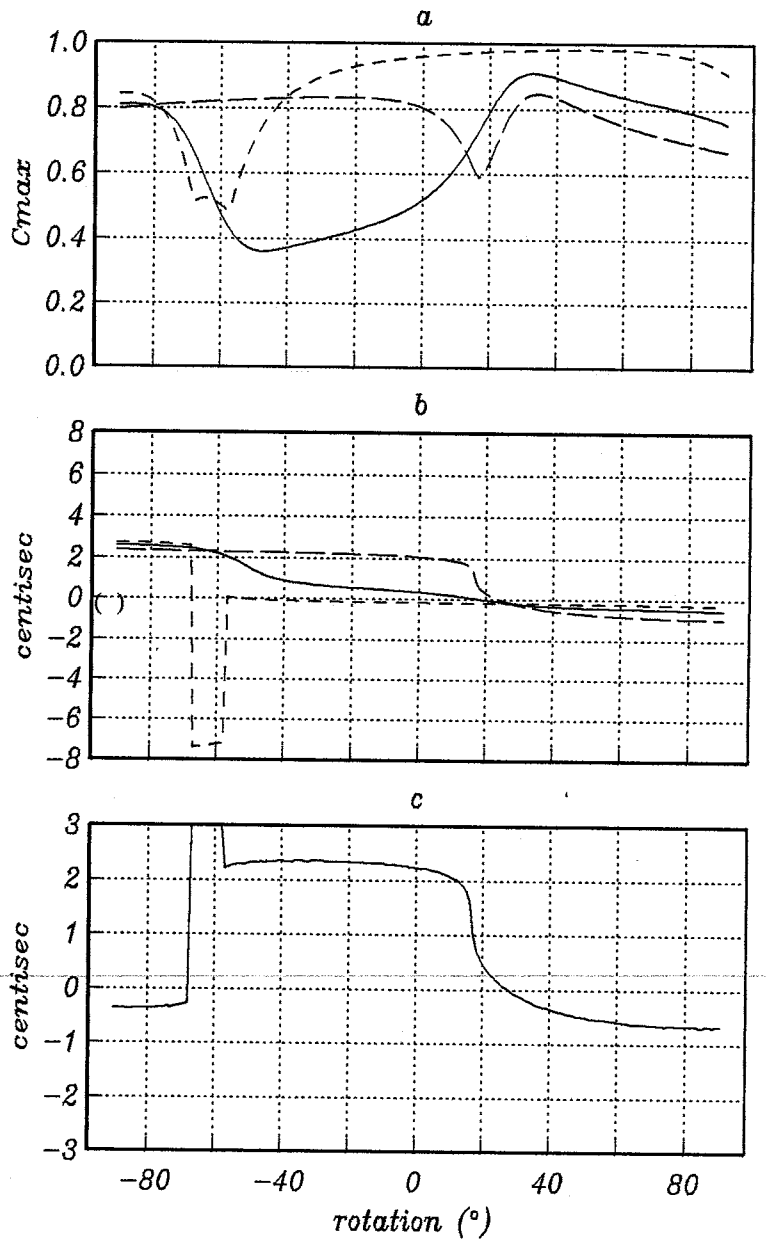

Figure 7. Shear wave cross-correlations as a function of lag time and coordinate system rotation for the similar event pair of Figure 7 recorded at EWC. After initially rotating both events to the quasi-fast shear wave (S_{fast}), quasi-slow shear wave (S_{slow}) ($N7.5°E$) coordinate system of the 1992 event, we rotated the coordinate system of the 1995 event clockwise from −90° to 90° and calculated the cross-correlation across the horizontal components in a 16 sample window. For (a) and (b) the short, dashed line is the S_{fast} polarization cross-correlation maximum, the long, dashed line is the S_{slow} polarization cross-correlation maximum, and the solid line represents the composite cross-correlation maximum of both components. (a) Peak cross-correlation of each component and the composite cross-correlation functions across each horizontal pair. (b) Lag time (10^{-2}sec) at maximum cross-correlation for each of the curves in (a). (c) Difference in shear-wave splitting times (10^{-2}sec) of the events as function of rotation angle, as estimated by the difference in lags between the S_{fast} and S_{slow} components.

Figure 7c. Notice that the composite cross-correlation peak (Figure 7a) coincides very closely with the zero-crossing of the differential lag curve (Figure 7c), suggesting that when the coordinate systems are properly aligned there is no detectable change in anisotropy orientation or magnitude between the July 26, 1992 and August 12, 1995 microearthquakes, despite the occurrence of the Landers earthquake during the intervening interval. Analyzing the P-waves of this similar event pair in the same fashion (Figure 8) results in maximum peak composite cross-correlation when the coordinate system of the 1995 event is rotated 21° to the west - roughly consistent with previous calculations based on P-wave initial particle motion of $M_l \geq 3.5$ earthquakes in the area and with the shear-wave differential analysis of the similar event pair. The consistency of rotation direction and magnitude for P and S waves is further evidence that a mere instrumental coordinate system change has occurred after the Joshua Tree-Landers sequence, rather than a change in the anisotropic crustal characteristics.

We summarize the differential analysis results of all four pairs spanning the Landers earthquake and the horizontal coordinate system reorientation in Table 2. The three additional pairs to the example pair discussed, are consistent in rotation direction and magnitude and differential splitting time, $\Delta\tau$. With the applied correction, the clockwise rotation of the fast shear-wave azimuth, $\overline{\Delta\theta}$, is $(1.5 \pm 7°)$ and the change in splitting time, $\overline{\Delta\tau}$, is $2.9\times10^{-3} \pm 2.1\times10^{-3} s$. The mean westward rotation is insignificant considering the large standard deviation. The mean differential shear-wave splitting time, $\overline{\Delta\tau}$, is subsample even at one standard deviation.

We were also able to constrain the time period from April 4, 1994 through January 22, 1996 using a fifth pair of similar microearthquakes with a high cross-correlation (0.802) at EWC. This pair of

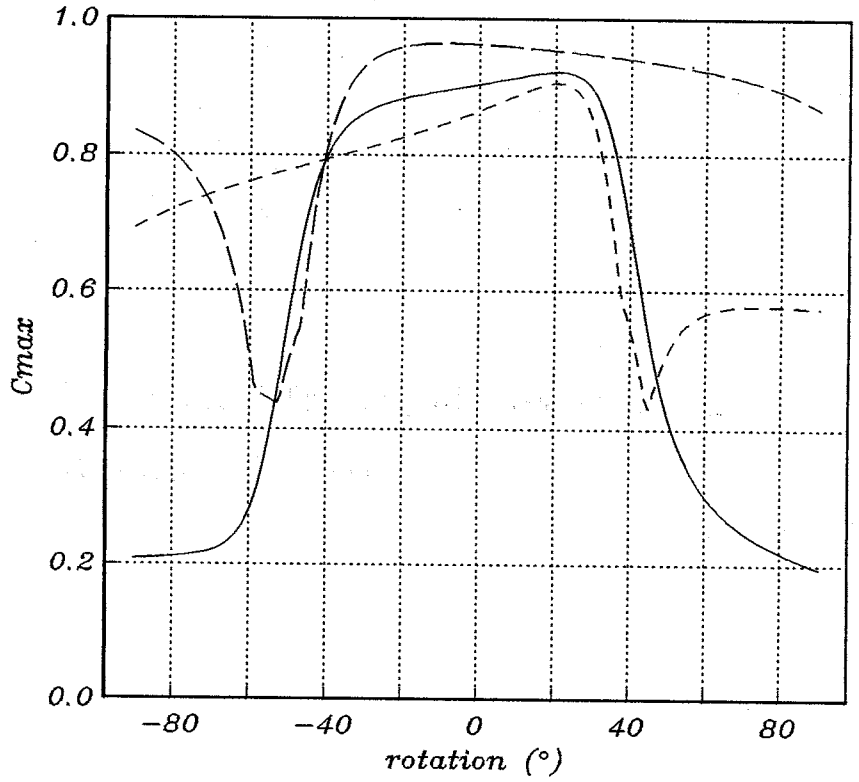

Figure 8. Cross-correlation analysis performed on the EWC P wave (16 samples beginning at the P pick) horizontal components of the similar event pair while clockwise rotating the horizontal components of 1995 event relative to the 1992 event. The short, dashed line is the S_{fast} polarization cross-correlation maximum, the long, dashed line is the S_{slow} polarization cross-correlation maximum, and the solid line represents the composite cross-correlation maximum of both components.

events has relatively noisy traces at other stations and therefore has a low median peak cross-correlation across the network. We applied the previously described differential analysis and found a peak in the composite S-wave cross-correlations when the 1996 event's coordinate system is rotated 3° east of the 1994 event's coordinate system. The magnitude of the rotation shows the stability of the horizontal components. Differential shear-wave splitting time at the rotation of maximum similarity of the S-wave is again nearly zero ($3.125\times10^{-4}s$), indicating no detectable

changes in crustal shear-wave anisotropy during the time interval spanned by this similar microearthquake pair.

Another useful way of observing the results of the application of the 33° correction to the 1995 is to compare directly the seismograms from the uncorrected 1995 event (Figure 9a) with those of the 1992 event (Figure 9c). Both events have been rotated to the S_{fast}, S_{slow} coordinate system

Table 2: Differential Analysis

Pair	Date of events	Rotation based on P (°)	Peak composite P cross-correlation	Rotation based on S (°)	Peak composite S cross-correlation	apparent westward rotation with correction applied (°)	Δτ at median P rotation angle (10^{-2} sec)
A	6/26/92 8/12/95	21	0.927	33	0.857	12.5	0.531
B	5/13/92 10/31/94	5	0.593	16	0.910	-4.5	0.375
C	5/7/92 4/29/94	20	0.928	16	0.930	-4.5	0.297
D	6/15/92 9/20/94	22	0.823	23	0.903	2.5	-0.0469
		median = 20.5		median = 19.5°		mean = 1.5 ± 7	mean = 0.29 ± 0.21

of the 1993 event ($N7.5°E$). A change in lag time seems obvious, however after applying a correction to the 1995 event for the inferred seismometer rotation (Figure 9b) the apparent change in lag time disappears, accompanied by an increased similarity in the S_{fast} and S_{slow} components between the events. Although the initial portion of the 1995 event's corrected quasi-slow component is not very similar to the 1992 event's quasi-slow component (possibly due to noise), the rest

of the waveform shows the stability of the shear wave splitting time. To comprehensively compare the slow and fast components of each pair, the coordinate system of the later event must be rotated to the median rotation correction angle of 21°. Visually comparing a longer window of the horizontal component records (Figure 10), containing the P and S arrivals, illustrates the event pair similarity increases with the application of the 33° correction to the 1995 event.

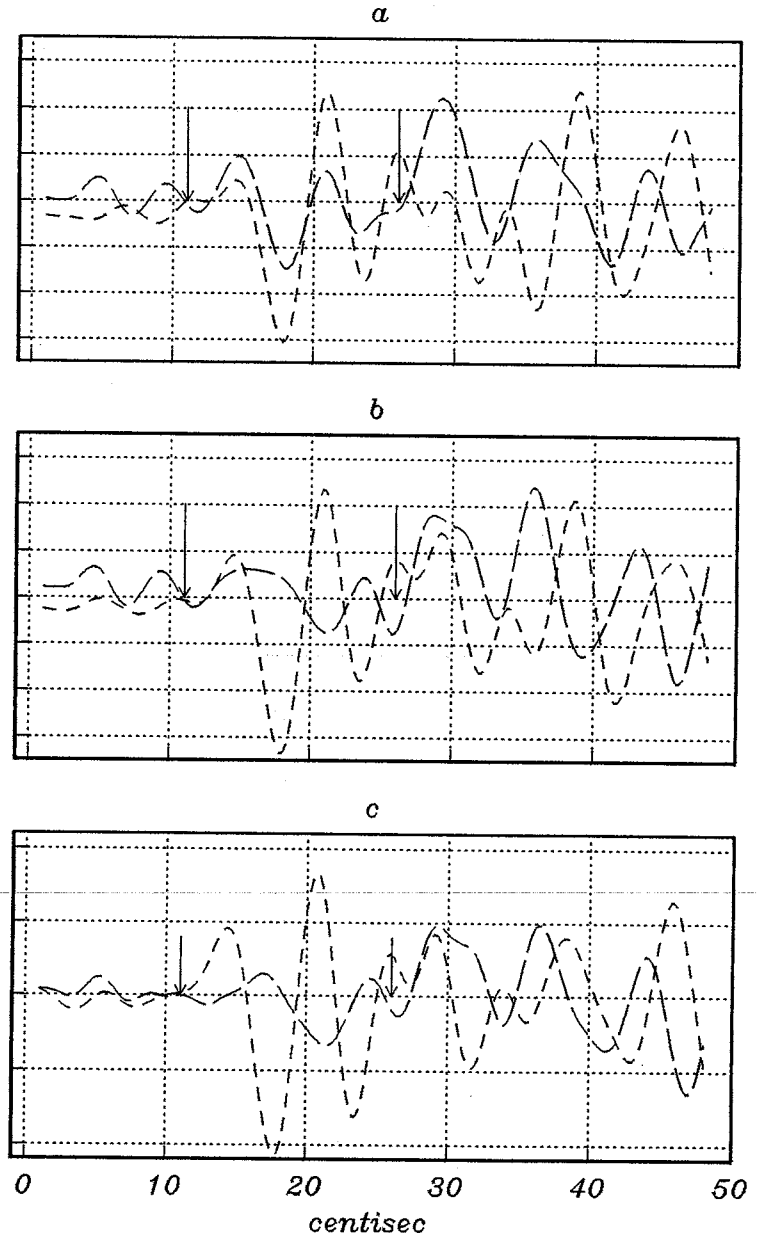

Figure 9. Quasi-fast and quasi-slow shear wave visual comparison for the example similar earthquake pair. The black arrows show the 16 sample cross correlation time window. All plots have been rotated to the 1992 events S_{fast},S_{slow} coordinate system ($N7.5°E$). (a) The 1995 event plotted uncorrected. (b) 1995 event with the application of the 33° correction for the inferred rotation correction. (c) 1992 event.

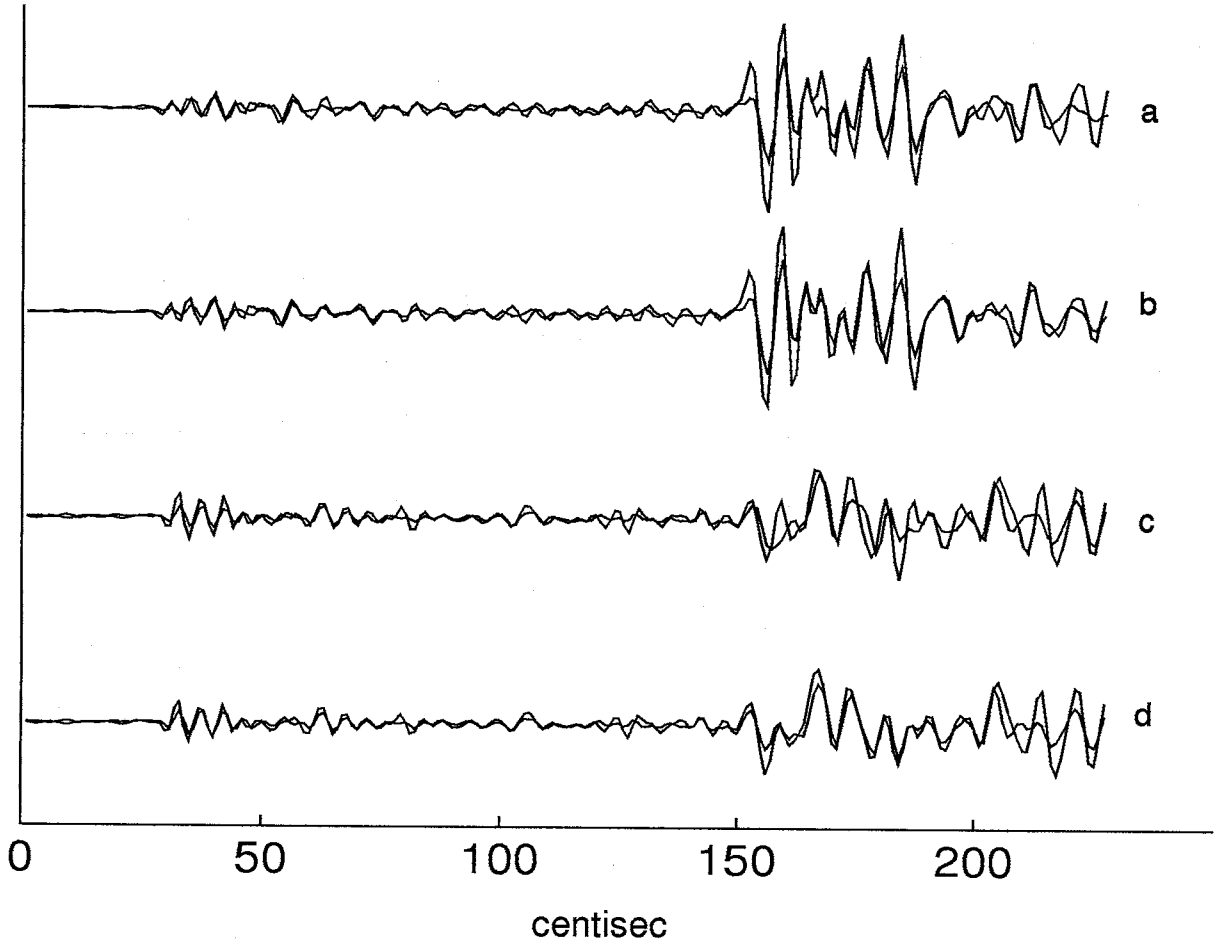

Figure 10. Overlay of horizontal components of the similar event pair with and without the rotation correction of 21° applied to the 1995 event. (a) "north" component of the 1995 event and the north component of the 1992 event. (b) corrected "north" component of the 1995 event and the north component of the 1992 event. (c) "east" component of the 1995 event and the east component of the 1992 event (d) the corrected "east" component of the 1995 event and the east component of the 1992 event. Notice the improved similarity on the S arrival and S-coda in (b) over (a). Improvements in similarity of (d) over (c) also exist in the P-arrival, P-coda, S-arrival, and S-coda.

Discussion and Conclusion

The inferred rotation of the horizontal coordinate system can be attributed to an undocumented change in seismometer orientation of 21° to the west, which changed the N-component orientation from $14°E$ to $7°W$ of true N. Station records indicate 3 station site visits between the two events. Two visits were of routine nature, however another (listed only on handwritten records) involved moving the seismometers a few meters. It is quite possible that the orientation of the seismometers was indeed changed during this move. Under SCSN protocol, seismometer orientations were not kept in station records (Wald, pers. commun.), other than in the naming convention (i.e. vertical, north, east). Verification of the seismometer orientation before the move on July 16, 1993 is thus not possible. Verification of the seismometer orientation after the move on July 16, 1993 is also not feasible as the station was shutdown and moved approximately 3km to the west (renamed EW2) (Wald, pers. commun.) on 2/15/96. A weak trend of eastward rotation of shear-wave initial particle motion (Figure 4) is evident even after considering the rotation correction (Figure 6), however analysis of the similar microearthquake pair (E) occurring after the horizontal component reorientation shows that shear-wave anisotropy characteristics remain stable during this time period.

I conclude that shear-wave anisotropy with a stable quasi-fast shear-wave has an orientation of $14°E$ of true N beneath station EWC. The largest earthquake sequence to occur in California in over 40 years, with an estimated 35 bar stress drop and over 70 km of surface rupture, did not affect crustal shear-wave anisotropy at detectable levels over timespans of 2-3 years, approximately 17 km south of the Landers surface rupture and less than 5 km from the Joshua Tree epicenter. I can constrain the pre-and co-seismic changes associated with the Joshua Tree earthquake

only by considering event by event analysis, due to the lack of seismicity prior to the Joshua Tree earthquake. I can only conclude that shear-wave initial polarization azimuths remained relatively stabile during the time period defined by the few events prior to Joshua Tree earthquake and after-shock activity of the Joshua Tree earthquake, considering the significant scatter in the initial polarization azimuths of Joshua Tree aftershocks and the lack of foreshocks. Finally I conclude that apparent post-seismic change in shear-wave anisotropy associated with the Landers earth-quake sequence observed in our study area is not crustal in nature.

Acknowledgments

The author thanks R. Aster for his support, encouragement, and insight. The linearity calculation and differential analysis code was written by R. Aster and is the core of this study. D. Dodge's assistance with the Xadjust and Velest programs is greatly appreciated. This research was funded by United States Geological Survey National Earthquake Hazards Reduction Program grant 1434-92-G-2627.

References

Antolik, M., R. M. Nadeau, R. C. Aster, T. V. McEvilly, Differential analysis of coda Q using similar microearthquakes in seismic gaps Part 2: application to seismograms recorded by the Parkfield High Resolution Seismic Network, *Bull. Seismol. Soc. Am.*, in press, 1996.

Aster, R. C., P. M. Shearer, and J. Berger, Quantitative measurements of shear wave polarizations at the Anza Seismic Network, southern California: implications for shear wave splitting and earthquake prediction, *J. Geophys. Res.*, 95, 12449 - 12472, 1990.

Aster, R. C., P. M. Shearer, High-frequency borehole seismograms recorded in the San Jacinto Fault Zone, southern California Part 1:Polarizations, *Bull. Seismol. Soc. Am.*, 81, 1057-1080, 1991a.

Aster, R. C., P. M. Shearer, High-frequency borehole seismograms recorded in the San Jacinto Fault Zone, southern California Part 2. Attenuation and site effects, *Bull. Seismol. Soc. Am.*, 81, 1081-1100, 1991b.

Aster, R.C., G. W. Slad, J. Henton, M. Antolik, Differential coda Q using similar microearthquakes in seismic gaps Part 1: Techniques and application to seismograms recorded in the Anza seismic gap, *Bull. Seismol. Soc. Am.*, in press, 1996.

Atkinson, B. K., A fracture mechanics study of subcritical tensile cracking of quartz in wet environments, *Pure Appl. Geophys.*, 117, 1011-1024, 1979.

Bennett, R. A., R. E. Reilinger, W. Rodi, Y. P. Li, M. N. Toksoz, K. Hudnut, Coseismic fault slip associated with the 1992 M_w=6.1 Joshua Tree, California, earthquake: implications for the Joshua Tree Landers earthquake sequence, *J. Geophys. Res.*, 100, 6443-6461, 1995.

Booth, D.C. and S. Crampin, Shear wave polarizations on a curved wavefront at an isotropic free-surface, *Geophys. J. R. Astron. Soc.*, 83, 31-45, 1985.

Campbell, K. W. and Y. Bozorgina, Empirical analysis of strong ground motion from the 1992 Landers, California, Earthquake, *Bull. Seismol. Soc. Am.*, 84, 573-588, 1994.

Crampin, S., Seismic-wave propagation through a cracked solid: polarization as a possible dilatancy diagnostic, *Geophys. J. R. Astron. Soc.*, 53, 467-496, 1978.

Crampin,S., R. Evans, B. Ucer, M. Doyle, J. P. Davis, G. V. Yegorkina and A. Miller, Observations of dilatancy-induced polarization anomalies and earthquake prediction, *Nature*, 286, 874-877, 1980.

Crampin, S., R. Evans, and B. K. Atkinson, Earthquake prediction: a new physical basis, *Geophys. J. R. Astron. Soc.*, 76, 147-156, 1984.

Dodge, D. A., G. C. Beroza, Foreshock sequence of the 1992 Landers, California earthquake and its implications for earthquake nucleation, *J. Geophys. Res.*, 100, 9865-9880, 1995.

Ellsworth, W. L., Three-dimensional structure of the crust and mantle beneath the island of Hawaii, 327 p., Ph.D. thesis, Mass. Inst. of Technol., Cambridge, 1977.

Gupta, I. N., Dilatancy and premonitory variations of P, S travel times, *Bull. Seismol. Soc. Am.*, 63, 1157-1161, 1973a.

Gupta, I. N., Premonitory variations in S wave velocity anisotropy before earthquakes in Nevada, *Bull. Seismol. Soc. Am.*, 182, 1129-1132, 1973b.

Hafner, K., R. Clayton, Southern California Earthquake Center user manual, 1994.

Hauksson, E., L. M. Jones, K. Hutton, and D. Eberhart-Phillips, The 1992 Landers Earthquake Sequence: Seismological Observations, *J. Geophys. Res.*, 98, 19835-19858, 1993.

Kanasewich, E., *Time Sequence in Analysis in Geophysics*, University of Alberta Press, Edmonton, 1975.

King, G. C. P., R. S. Stein, J. Lin, Static stress changes and the Triggering of Earthquakes, *Bull. Seismol. Soc. Am.*, 84, 935-953, 1994.

Lachenbruch A. H. and Sass J. H., Heat-flow from Cajon Pass, fault strength, and tectonic implications, *J. Geophys. Res.*, 97, 4995-5015, 1992.

Munson, C. G., C. H. Thurber, Y. Li, P. G. Okubo, Crustal shear wave anisotropy in southern Hawaii: spatial and temporal analysis, *J. Geophys. Res.*, 100, 20367-20377, 1995.

Nadeau, R. M., W. Foxall, T. V. McEvilly, Clustering and periodic recurrence of microearthquakes on the San Andreas Fault at Parkfield, California, *Science*, 267, 503-507, 1995.

Nur, A., Dilatancy, pore fluids, and premonitory variations of T_s/T_p travel times, *Bull. Seismol. Soc. Am.*, 62, 1217-1222, 1972.

Nur A. and Byerlee, J. D., An exact effective stress law for elastic deformation of rock with faults, *J. Geophys. Res.*, 76, 6414-6419, 1971

Nur A. and G. Simmons, Stress-induced velocity anisotropy in rock: an experimental study, *J. Geophys. Res.*, 74, 6667-6674, 1969.

Savage, M. K., X. R. Shih, R. P. Meyer, and R. C. Aster, Shear-wave anisotropy of active tectonic regions via automated s-save polarization analysis, *Tectonophysics*, 165, 279-292, 1989.

Scholtz, C. H., *The mechanics of earthquakes and faulting*, Cambridge University Press, Cambridge, U.K., 1990.

Sieh, K., et al., Near-field investigations of the Landers earthquake sequence, April to July 1992, *Science*, 260, 171-175, 1993.

Vázquez-Contreras, A., D. C. Booth, F. R. Zúñiga, E. Chesnokov, S. Crampin, and R. Meisnner, Seismic anisotropy in the Guerrero Gap, Mexico: preliminary results, *Geophys. Res. Lett.*, 20, 69-72, 1993.

Whitcomb, J. H., J. D. Garmany, and D. L. Anderson, Earthquake prediction: variation of seismic velocities before the San Francisco earthquake, *Science*, 180, 632-635, 1973.

Zoback, M. D., et al., New evidence on the state of stress of the San Andreas fault system, *Science*, 238, 1105-1111, 1987.

List of Appendices

Appendix A. Accessing data at SCEC.....3 pages

Appendix B. Obtaining hypocenter relocations.....5 pages

Appendix A

For this section menu options are underlined, directories and paths are in single quotes, executables are in bold, and files are italized.

This appendix shows how to obtain data from the SCEC database. The process is as follows:

1. Create a search request file.
2. Run **retrieve_data.**
3. Ftp data to New Mexico Tech.

1. As an example of a search request file I present a file used to find events within the conical search volume.

To acquire data within the conical search volume, I had to approximate a cone with stacked, short cylindrical volumes, analogous to a layered wedding cake. I show the file, *scsn.req.ewc.2-4*, read by the SCEC sorter program, **dbsort**, used to search for events within the layer, 2-4 km in depth (All scripts, files, and data discussed here at SCEC reside in /export/scec/user1/aster/Datastrip/Landers).

File: *scsn.req.ewc.2-4*	Setting meaning
verbose=3	print final search summary, search window, and event information
eventqual=A	horizontal location error < 1.0 km, vertical location error < 2.0 km
eventtype=L	local events
date1=810101	start on 1/1/81
date2=990101	end on 1/1/99
depth=2,4	hypocenters between 2 and 4 km
distmax=2.8	outer search radius of 2.8 km
output=scsn.out	list of events found in search
dogram=1	extract waveforms

dophase=1	extract phase information
station=EWC	use EWC as the center of this search
network=SCSN	SCSN network stations

For a complete listing of variables that dbsort can search on, type dbsort at the scec prompt.

A file similar to one shown exists for each 2 km depth segment of the conical search volume.

2. A shell script, originally written by R. Aster, **retrieve_data,** calls **dbsort**, pulls the waveforms in SAC format, places the SAC files in subdirectories based on event id, creates a tarfile of the data, and compresses the tarfile. In the case of the cone, an additional script, **run_retrieve**, calls **retrieve_data** for each layer, assuming a valid request file exists for each layer.

The script **retrieve_data** takes the input file name immediately following it on the command line. The script used pull of the entire cone dataset, **run_retrieve**, requires nothing else on the command line after it.

3. Transfer the data to New Mexico Tech via FTP.

Below I show a session in which events within the 2-4 km depth layer are searched for, collected, and transferred via FTP.

```
griffy> rlogin -l aster scec
/export/scec/user1/aster/Datastrip/Landers
Password:
scec{aster}1: cd Datastrip/Landers
scec{aster}2: retrieve_data scsn.req.ewc.2-4
```

executing dbsort request
retrieving seismograms
creating the data directories
removing unwanted SAC files
removing empty data directories
scec{aster}3: ftp griffy.nmt.edu
Connected to griffy.nmt.edu.
220 griffy FTP server (SunOS 4.1) ready.
Name (griffy.nmt.edu:aster): fgb
331 Password required for fgb.
Password:
230 User fgb logged in.
ftp> cd /mk2/fgb/EWC
250 CWD command successful.
ftp> put tarfile.Z
200 PORT command successful.
150 ASCII data connection for tarfile.Z (131.215.61.1,3042).
226 ASCII Transfer complete.
local: tarfile.Z remote: tarfile.Z
1822897 bytes sent in 3.6e+02 seconds (4.9 Kbytes/s)
ftp> quit
221 Goodbye.
scec{aster}4: logout
Connection closed.
griffy>

Appendix B

For this section menu options are underlined, directories and paths are in single quotes, executables are in bold, and files are italized.

The microearthquake relocation process can be broken down into 3 phases.

Phase 1. Sac format waveforms are preprocessed before analysis. Waveforms are checked for minimum energy level, event distance from station, sampling rate, reference time, and frequency content. If picks do not exist for a waveform, initial picks are made. Waveforms suitable for further analysis are placed into directories corresponding to the station that recorded the trace.

Phase 2. Arrivals are repicked using **Xadjust**. Waveforms are analyzed station by station. The windowed waveform most similar to the rest of the waveforms is placed on top of the list, with events decreasing in similarity to this master event displayed in descending order. Waveforms are placed in groups based on similarity. A pick from each group is held fixed while the remaining picks within each group are adjusted based on waveform similarity to the master trace within each group. Sac header variables are readjusted to reflect the new picks.

Phase 3. The repicked events are input into mkinfile, a routine that processes the repicked events into a format suitable for the inverstion program **VELEST**. **VELEST** inverts first for hypocenter location and depth and a revised velocity model. With a new velocity model, **VELEST** inverts a second time for hypocenter location and depth, holding the velocity model constant. A final program **velout2xyz2** outputs the errors associated with each hypocenter loca-

tion.

All preprocessing, repicking, and relocating are done in the directory '/mk2/fgb/EWC/preprocess', subdirectory of '/mk2/fgb/EWC/preprocess', or '/home/src/velest'.

Phase 1

1. Move the SAC files from all of the event directories to '/mk2/fgb/EWC/preprocess/'. Run **makelist** to create a list, named *tmp*, of cuspids of all events.

2. The FORTRAN program **preprocess** screens out the vast majority of unsuitable traces, based on parameters set in the *preprocess.ini* file. A strict adherence to the naming convention of traces is required by **preprocess**. The naming convention used to pull data over from SCEC is cuspid.station.component.SAC. The format required for preprocess does not have a period between cuspid and station (i.e. 123456EWC.VHZ.SAC, rather than 123456.EWC.VHZ.SAC). The tc-shell script **rename**, drops the first period of all sac files in the directory it is executed in. Run **rename**.

3. A tc-shell script, **preprocessor**, calls the FORTRAN program **preprocess** on all cuspids in the file *tmp*. Run **preprocessor**. After **preprocessor** has finished, all suitable traces will be in the appropriate station directory. Problematic traces may fall into one of the following directories: 'Badfile', 'NoDBentry', 'BadComp', 'RefTime', MaxDist', 'AbsVal', 'AvMax', 'Freq', or 'PickBounds'. The default parameters within *preprocess.ini* (brief descriptions of the parameters are included in *preprocess.ini*) yield satisfactory results for the EWC cone dataset, however depending on the individual dataset, certain parameters within the preprocess.ini file may be adjusted to maximize the number of traces suitable for additional processing with **Xadjust**.

Phase 2

1. Station by station traces are sorted by similarity. **Xadjust** resides in the 'preprocess' directory. Start MATLAB and the type **Xadjust** at the matlab prompt.

2. Under the File menu, choose Set Input Data. The default path is the current path Matlab is running in. Include the station directory in the path. Click on Apply.

3. Under the File menu, choose Read Seismograms. The window opening up contains all the traces (up to 40 viewable at one time, use the scroll bar to see additional traces) from the station input earlier. Examine the traces, if any cuspids do not have an associated trace, delete these now using the delete button.

4. Under the Parameters menu, choose Cross Correlation window. Set the Window Pre-Pick Secs. to -0.5s and Window Post-Pick Secs. to 1.0s.

5. Within the Auto Adjustment menu, Click on Sort Traces Around P. Traces are sorted based on similarity, the most similar trace to the entire group is placed on top, with traces listed in descending similarity to the master trace.

6. Under the Auto Adjustment menu, choose LS Adjust P. Traces are grouped by color into clusters similar to each other.

7. Under the Auto Adjustment menu, chose Adjust All P Groups. A window opens, displaying, a group at a time, up to 3 traces with the most identifiable picks. Choose the least ambiguous pick for each group and click Next to advance to the next group of seismograms. An 'X' appears as the pick when the last group is redisplayed after choosing Next, then exit this mode by clicking on Close. Within each group picks are adjusted to obtain maximum a maximum peak cross-correlation relative to the pick fixed with in each group.

8. Within the Main Trace Display menu, choose Refresh Display. Visually inspect the picks, using the Zoom option if necessary. To use the Zoom option hold the left mouse button down and box in the desired seismograms and/or seismogram segments. Cycle skipping may occur and is quite often obvious. Correct obvious erroneous picks, using the Move P, button and adjust errors bars accordingly using the Set P Error button under the Manual Adjustment menu buttons. After completing the pick inspection, save the picks. Some experimentation with the parameters, may improve group size, traces included in groups, and/or reduce the occurrence of cycle skipping, depend on individual datasets.

9. Repeat steps 2-9 for each station directory, until all station directories have been processed. After processing all stations, exit Xadjust through the File menu choosing Exit.

Phase 3

1. Move all the sac files in each station directory into a directory named '/Invert/Complete/'. A FORTRAN program, **mkinfile**, reads the sac files from the '/Invert/Complete/' directory and formats the event information into a **VELEST** readable format. The output of **mkinfile** sends its output to velest.infile. Within the source code of **mkinfile**, the minimum number of stations required for an event to be inverted (currently set at 5 stations) maybe adjusted. Run **mkinfile**.

---

2. **VELEST** and associated files live in 'preprocess/Invert'. Edit the command file, velest.cmn, and set the following variables accordingly:

Input variables and files:

neqs = number of earthquakes in velest.infile
isingle = 0
invertratio = 0
istaout = 2

modelfile = *landers.hauks.mod*
Stationfile = *landers.sta*
File with Earthquake data = *velest.infile*

Output variables and files:

Main print output file = *landers.out.ex*
File with final hypocenters in *.cnv format = *landersout.CNV.ex*
File with new station corrections = *landers.sta.ex*
File with raypoints = *rays.out.ex*
File with residuals = *velout.res.ex*

As set above, **VELEST** will jointly invert for a revised velocity model and hypocenter location and depth. Run **VELEST**.

3. After the first inversion, change the following variables in the *velest.cmn* file.

Input files:

neqs = 1
isingle = 1
invertratio = 0
istaout = 1
modelfile = *velout.mod*
File with Earthquake data = velest.infile (file with similar event pairs in proper format)

Output files:

Main print output file = *landers.out.ex.pairs*
File with final hypocenters in *.cnv format = *landersout.CNV.ex.pairs*
File with raypoints = *rays.out.ex.pairs*
File with residuals = *velout.res.ex.pairs*

4. Create a *velest.infile* with only the similar microearthquake pairs. Run **VELEST** on shelflife.

A parameter within the source code is hard-wired to read certain files from '/home/SRC/velest'. The appropriate files are installed in '/home/SRC/velest' on shelflife.

5. The FORTRAN program, **velest2xyz2**, computes the 2σ errors in location of each event. Run **velest2xyz2**, redirecting the standard out to a file.